Static and Dynamic Stress/Strain Properties for Human and Porcine Eyes

Katherine D. Voorhies

Thesis submitted to the Faculty of the Virginia Polytechnic Institute and State University in partial fulfillment of the requirements for the degree of

Master of Science
in
Mechanical Engineering

Stefan Duma, Chair
Elaine Scott
Ian Herring

April 22, 2003
Blacksburg, VA

Keywords: Eye, Stress, Strain, Biomechanics

Static and Dynamic Stress/Strain Properties for Human and Porcine Eyes

Katherine D. Voorhies

(ABSTRACT)

Every year, more than 2.4 million eye injuries occur in the United States, with over 30,000 of those injured left blind in at least one eye as a result. Computer modeling is one of the most versatile ways to study ocular trauma, however, existing models lack accurate stress and strain properties for ocular globe rupture. A pressure system was built to examine static and dynamic globe rupture pressures for healthy postmortem human and porcine (pig) eyes. Maximum rupture stress for the quasi-static tests was found to be 11.17MPa for human tissue and 12.08MPa for porcine tissue, whereas stress for the dynamic tests was found to be 30.18MPa for human tissue and 26.01MPa for porcine tissue. Maximum rupture stress results correlate well with static material properties used in published research (9.4MPa), and dynamic properties of 23MPa found in published research. Healthy postmortem human eyes were ruptured statically and dynamically to determine the relationship between stress and strain for the ocular globe under intraocular pressure loading. Stress-strain relationships were investigated and values for the elastic modulus were found to be slightly lower than that previously published. This research shows that it is important to differentiate between tissue type, and static versus dynamic failure properties before drawing conclusions from computer models and other published research. Now that rupture can be accurately determined, safety systems designed to protect eyesight in automotive, sports, and military applications can also be applied to protect the quality of life for humans in these applications.

Static and Dynamic Stress/Strain Properties for Human and Porcine Eyes

Table of Contents

List of Tables and Figures

CHAPTER 1

Objectives

The objective of this work is to discover, experimentally or computationally, pressure and rupture strength limitations of the globe, as well as stress-strain relationships of the globe.

Introduction

Every year, more than 2.4 million eye injuries occur in the United States, with over 30,000 of those injured left blind in at least one eye as a result (Biehl, 1999; Parver, 1986). Financial, emotional, and societal issues are just some of the potentially debilitating problems brought on by impaired sight and blindness. Over the past few decades, safety systems in sports, automotive, and military applications have greatly improved, decreasing life-threatening injuries. Because humans are more likely to live through traumatic events, less threatening injuries, such as ocular injuries, become more apparent. A number of studies have been published analyzing the effect of sports, automotive, and military trauma on eyes (Bass, 2002; Biehl, 1999; Chisholm, 1969; Doswald-Beck, 1993; Duma, 1996; Ghafouri, 1997; Heier, 1993; Muller-Jensen, 1970; Power, 2002; Stein, 1999; Vichnin, 1995; Vinger, 1999).

One of the most inexpensive, versatile ways to analyze injuries of any kind is computer modeling. A few ocular computer models have been created, but most have been designed to study corrective eye surgery and are only accurate for static solutions (Bryant, 1996; Hanna, 1989; Sawusch, 1992; Wray, 1994). Three models have been used for dynamic events, with the most up to date and accurate model being the Virginia Tech Eye Model (VTEM) created by Stitzel (2002). Previously, uniaxial tensile strip tests were performed on the sclera and cornea for the first dynamic computer model presented by Kisielewicz (1998) and Uchio (1999). However, for accurate rupture stress and strain, material properties obtained in a more lifelike situation are desirable. In a living human, globe stress and strain are not uniaxial, and anatomical ocular components will affect the results of globe strength and expansion. Because the computer models to date are unable to show rupture (rupture must be inferred based on stress results), it is imperative to have accurate properties for injury criteria. Uchio (1999) found peak rupture stress using static material properties to be 9.4MPa, whereas the VTEM, with more realistic dynamic modeling, found peak rupture stress to be 23MPa (Stitzel, 2002). The VTEM was experimentally verified and is currently the state of the art in ocular computer models. Unfortunately, existing models all lack accurate stress and strain properties for rupture of the ocular globe, which is one of the most important properties needed to analyze overall strength of the eye.

Additionally, safe intraocular pressures are of particular interest to the clinical ophthalmologist, who may not be aware of the upper range for intraocular pressures before the eye would rupture. In published research, rupture pressure of eyes has been examined to determine the effect of ocular surgery, but no studies have been published on the rupture pressure of healthy human eyes. Burnstein (1995) studied the strength of

postmortem human and porcine eyes after undergoing photorefractive keratectomy by increasing intraocular pressure (IOP) gradually with nitrogen gas until globe rupture occurred. By testing rupture of 7 porcine eyes that had undergone photorefractive keratectomy, Burnstein found rupture pressures between 0.345MPa (50psi) and 0.621MPa (90psi). In testing only human anterior segments for corneal integrity after refractive surgery by raising intraocular pressure, Pinheiro (1995) found rupture pressures of approximately 1.240MPa with rupture occurring at the limbus or incision site. No experiments have been found where globe rupture was studied for the intent of learning properties of healthy postmortem eyes.

General Ocular Anatomy

The human eye is an incredibly complex anatomic structure (Figure 1). The globe is approximately 24.8 mm from anterior to posterior and 24 mm from superior to inferior poles. The eye is comprised of two main segments; the anterior segment, which is filled with aqueous humor, and the posterior segment, which is filled with vitreous. The lens and zonules form a boundary between the anterior and posterior segments. The crystalline lens changes shape through its elastic properties to refract light onto the retina at the back of the eye to form images that are transmitted to the brain for interpretation by the optic nerve. The lens itself is suspended in the intraocular fluid (aqueous humor and vitreous), and is focused through movement of the zonules and ciliary muscle. The cornea is the transparent structure covering the front of the anterior chamber. Although fine adjustments in focus are made by the changeable lens, most of the overall focusing power is maintained by the cornea.

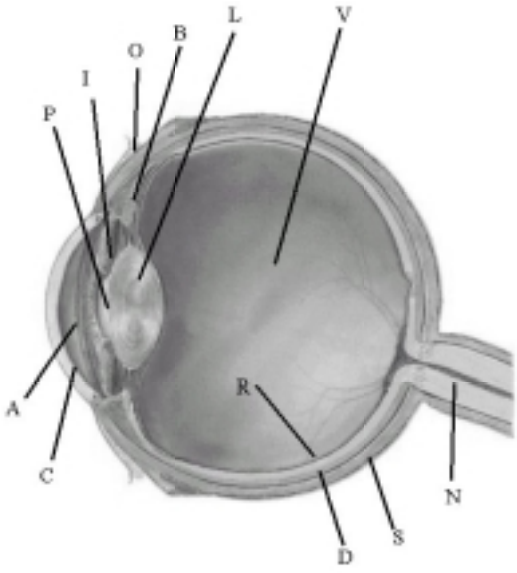

Figure 1 Ocular Anatomy: A) aqueous humor, B) ciliary body, C) cornea, D) choroid, I) iris, L) lens, N) optic nerve, O) conjunctiva, P) pupil, R) retina, S) sclera, V) vitreous humor

The cornea and sclera comprise the fibrous tunic (the outermost cover) of the eye. Although the cornea and sclera consist mostly of collagen fibers, the orientations of the fibers differ. The cornea collagen fibers are arranged parallel to each other in a regular

pattern, causing the cornea to be transparent. The sclera collagen fibers branch, and are not arranged regularly, causing the sclera to be opaque.

Ocular Surrogate Models

Fresh postmortem human eyes are difficult to obtain. Eyes can be procured from eye banks in the area, however first priority is given to the high demand for corneal transplants, severely limiting the quantity of eyes available for research. In addition, eyes are usually elderly, and cannot be obtained immediately postmortem because of mandatory disease testing. Many of the human eyes used in the included research were not fresh (up to 4 months old) but due to the limited availability of human eyes, all eyes obtained were used in the study. For results on fresher eyes, porcine eyes are also used in the research presented in this thesis.

An alternative to human and porcine eyes for ocular research is monkey eyes. Rhesus monkeys have proven to be quite similar to humans in their ocular makeup and presbyopic progression [Bito, 1982], and real-time in vivo study of the ocular components is possible with monkeys. Because we were performing destructive testing and postmortem testing for research, we did not need any rhesus monkeys for the experiments.

Porcine and Human Globe Rupture

Maximum stress of the ocular globe is an important property for injury criteria. However, studies including globe stress properties thus far have not used properties obtained from whole eye rupture tests under static and dynamic situations. Burnstein (1995) studied the strength of postmortem human and porcine eyes after undergoing photorefractive keratectomy when he ruptured eyes by increasing intraocular pressure (IOP) gradually with nitrogen gas until globe rupture occurred. The eye was attached to the nitrogen gas system by a 25-gauge butterfly needle that was inserted into the anterior chamber at the limbus. Pressure was increased by 5psi at 5-second intervals. Testing rupture of 7 porcine eyes, Burnstein found rupture pressures between 0.345MPa (50psi) and 0.621MPa (90psi) during rupture testing of eyes that had undergone photorefractive keratectomy, and rupture occurred at the equator in 6 of the 7 eyes. In 2 eyes undergoing phototherapeutic keratectomy, Burnstein found rupture pressures of 0.552MPa (80psi) and 1.24MPa (100psi). Testing only human anterior segments for corneal integrity after refractive surgery, Pinheiro (1995) found rupture pressures of approximately 1.24MPa with rupture occurring at the limbus or incision site. To the author's knowledge, no experiments have been reported where globe rupture was studied for the sole sake of learning properties of healthy postmortem eyes.

Studies have also been published analyzing the destruction caused by ocular injuries, such as baseball or BB impacts (Stitzel, 2002), or airbag testing in which researchers attempt to identify ocular injury scales and risk factors (Duma, 2002). Once the rupture stress is known for static and dynamic tests, the properties can be used to create safer guidelines for sports and automobile applications, and computational models will be

more accurate. Because ocular material properties, necessarily, are investigated using destructive tests, the eyes used are postmortem.

Stress-Strain Relationships

Very little information exists regarding the stress-strain relationship for the fibrous tunic of the human eye, and this information is critical when analyzing globe properties computationally. The nonlinear elastic modulus (E) values in the Virginia Tech Eye Model (VTEM) (Stitzel, 2002) were drawn from a published model presented by Uchio (1999). Uniaxial tensile strip tests were performed on the sclera and cornea for the first dynamic computer model presented by Kisielewicz (1998) and Uchio (1999), however, for accurate rupture stress, material properties obtained in a more lifelike situation are desirable. In a living human, globe stress is not uniaxial, and ocular components will affect the results of globe strength.

Methodology

A pressure system has been built to examine the quasi-static and dynamic rupture pressure for human and porcine eyes (Figure 2). Saline (0.9% NaCl) is the same osmolarity as the physiological fluid that naturally flows throughout the body and was used in this system to provide the most realistic environment for rupture testing. Human and porcine eyes were connected to the pressure system via tubing and a 16-gauge intravenous (IV) needle inserted through the optic nerve. A fluid-tight seal was formed around the optic nerve and needle by cinching a wire around the tissue. The entire system was pressurized with a nitrogen gas tank through a pressure regulator to a holding tank. Pressure built in the holding tank until the system was ready to fire, triggered by opening a 2-way solenoid valve supplied by ASCO (Florham Park, NJ). Located just past the solenoid valve was the saline holding area. Saline flowed through the tubing and needle into the eye. A sight gage was located just upstream from the pressure transducer, which sent pressure data to the computer for analysis. The pressure transducer (HKM-375-500G, Kulite Semiconductor, Leonia, NJ), used to measure rupture pressure, was rated to 500psi with a maximum pressure of 1000psi. The pressure transducer had a 425kHz natural frequency, and a 10VDC excitation was used to interface with Waveview for data collection. Video data of rupture was captured using a high-speed camera (Phantom 4, Vision Research, Inc., Wayne, NJ). The pressure transducer data and high-speed video were correlated so that pressure could be determined at the exact moment of rupture. Quasi-static testing was analyzed at 50 frames/second for the video, and 50Hz for pressure data to allow for collection of data over the entire long-term event. For dynamic testing, video was taken at 6000 frames/second and data was collected at 6000Hz.

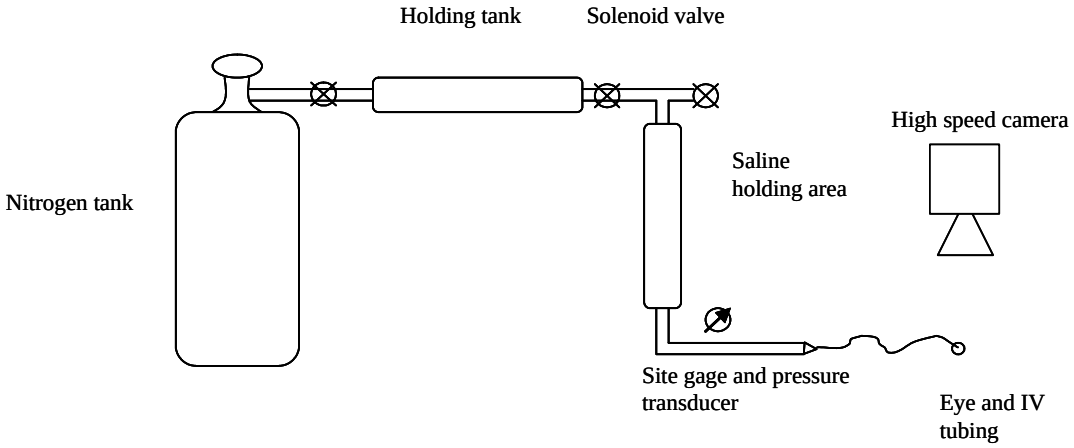

Figure 2 Schematic of pressure system used to examine quasi-static and dynamic rupture pressure for eyes

Stress

Healthy postmortem human and porcine (pig) eyes were used for the stress portion of the experiment (Table 1). Porcine eyes are commonly used as a surrogate during ocular research because they are similar to human eyes and are much easier to obtain (Duma, 2000). Human eyes were procured from the Roanoke Eye Bank (Roanoke, VA) where they were packaged in saline gauze and glass jars. Porcine eyes can be obtained immediately after slaughter. Since porcine eyes are so frequently used in ocular research, the potential differences in outcome based on differentiation of species and age are of interest in this experiment and are critical in ascertaining the clinical validity of ocular research using this surrogate model. Porcine eyes were procured from Animal Technologies (Tyler, TX) and were shipped to the testing location in saline with tissue attached.

Table 1 Test matrix for human and porcine eyes

	Human	**Porcine**
Static	10 eyes	10 eyes
Dynamic	10 eyes	10 eyes

Both quasi-static and dynamic testing was performed for this experiment (Figure 3). Quasi-static testing was accomplished by increasing the internal pressure of the eye by approximately 1psi/s. The loading rate for quasi-static testing was achieved manually so some variation naturally occurs in the loading rate. Quasi-static rupture testing was performed using 10 human and 10 porcine eyes. Dynamic testing was accomplished by setting the initial pressure to release at 2.70MPa (400psi), a value much higher than the eye could tolerate. In this way, the eyes ruptured at their maximum dynamic pressure almost immediately. Dynamically, 10 human and 10 porcine eyes were tested.

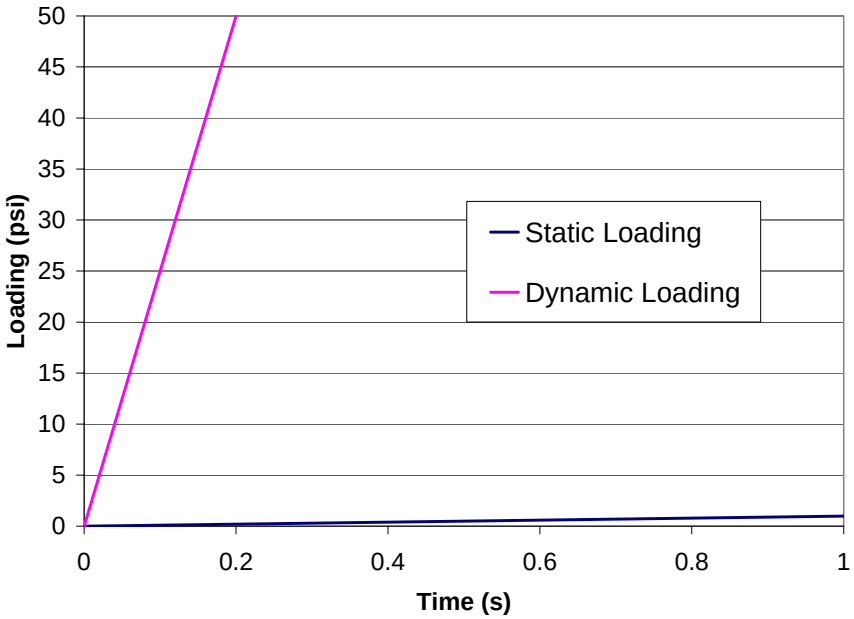

Figure 3 Loading rates for static and dynamic tests

For stress calculations (see Discussion) thickness and radius for each eye was needed. Thickness of eyes at the rupture location was accomplished with histology (Appendix I). Histology is a common method of preparing tissue for measurement; however, the actual process may introduce some artifacts in the size of the tissues (Young 2000). Currently, however, this is the most accessible way to measure tissues. Two human and two porcine eyes were examined. Globe radius, used in the stress calculations, was determined individually for each eye at the instant of rupture was based on the high-speed video footage (Figure 4) (Appendix H). Measuring tape was inserted into one of the tests and used to determine the relationship between the number of pixels on the video and the length in mm.

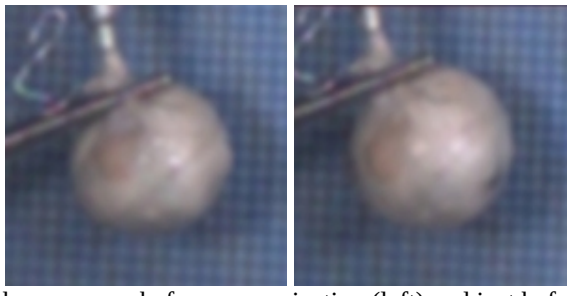

Figure 4 Globe expansion of the same eye before pressurization (left) and just before rupture (right)

Strain

Video of the entire pressurization event was reviewed for strain by determining the distance between key points on opposite edges of the eye. After finding the length to pixel ratio (Equation 1) by including a measuring tape in the video, pixel x- and y- values were recorded throughout the event for the predetermined locations on the eye. The

predetermined locations included points at the rear (near the optic nerve) and front of the eye (near the cornea). The length in pixels was then related to the length in inches.

$$44 \text{ pixels} = 1 \text{ in} \quad (1)$$

Healthy postmortem human eyes were used for the strain portion of this experiment (Table 2). The human eyes obtained were between 67 and 87 years of age and were tested at varying times after death (between 1 and 4 months post-mortem).

Table 2 Test matrix for stress-strain properties of human eyes

Human Eye	**Test Type**	**Age (years)**	**Time from Death (days)**
1	Static	67	33
2	Static	87	74
3	Dynamic	71	115
4	Dynamic	72	96

Results

Stress

Under static loading, rupture pressure for human tissue varied from 0.12MPa to 0.65MPa with the mean being 0.363MPa and, accordingly, rupture stress varied from 1.76MPa to 11.17MPa with the average being 5.34MPa. For porcine tissue, rupture pressure varied from 0.73MPa to 1.26MPa with the mean being 1.0MPa and, accordingly, rupture stress varied from 4.93MPa to 12.08MPa with the average being 9.38MPa (Table 3).

Table 3 Data for quasi-static rupture testing

Human					**Porcine**				
Test	Time to Rupture (s)	Rupture Pressure (MPa)	Globe Radius (mm)	Rupture Stress (MPa)	Test	Time to Rupture (s)	Rupture Pressure (MPa)	Globe Radius (mm)	Rupture Stress (MPa)
H009	40	0.35	11.7	2.82	P035	117	1.25	12.7	4.95
H010	12	0.12	12.2	1.76	P036	111	1.05	14.5	12.08
H011	98	0.48	13.1	7.47	P037	66	0.73	13.6	7.95
H012	24	0.15	13.0	2.30	P038	96	0.97	14.4	11.14
H013	58	0.29	13.6	4.59	P039	122	1.26	13.1	4.93
H020	20	0.22	14.1	3.73	P040	99	1.11	12.5	11.07
H021	26	0.64	14.7	11.17	P062	56	0.95	14.7	11.20
H023	27	0.52	14.9	9.16	P064	39	1.05	14.4	12.08
H024	33	0.65	16.2	7.23	P065	22	0.78	13.0	8.08
H026	14	0.21	13.3	3.21	P067	20	0.85	15.2	10.32
Average		0.36		5.34	Average		1.00		9.38
St. Dev.		0.20		3.21	St. Dev.		0.18		2.75

Rupture pressure for dynamic tests was much higher than the rupture pressure of the static tests. For human tissue, rupture pressure varied from 0.68MPa to 1.7MPa with the mean being 0.91MPa and, accordingly, rupture stress varied from 6.59MPa to 30.18MPa with the average being 12.81MPa. For porcine tissue, rupture pressure varied from

1.06MPa to 2.18MPa with the mean being 1.64MPa and, accordingly, rupture stress varied from 7.12MPa to 26.01MPa with the average being 14.43MPa (Table 4).

Table 4 Data for dynamic rupture testing

Human					Porcine				
Test	Time to Rupture (s)	Rupture Pressure (MPa)	Globe Radius (mm)	Rupture Stress (MPa)	Test	Time to Rupture (s)	Rupture Pressure (MPa)	Globe Radius (mm)	Rupture Stress (MPa)
H002	0.38	0.85	13.6	13.67	P048	0.47	1.06	15.4	13.08
H003	0.44	0.84	12.4	12.28	P049	0.68	1.75	14.8	7.71
H004	0.41	0.81	12.7	7.14	P054	0.77	1.61	17.3	22.31
H005	0.41	0.79	12.2	6.59	P055	0.61	1.51	14.3	17.31
H006	0.91	0.94	13.9	15.35	P056	0.58	1.78	13.4	7.12
H008	0.78	0.88	11.5	11.96	P057	0.41	1.34	12.1	12.99
H014	0.30	0.79	12.4	11.54	P058	1.35	1.91	17.1	26.01
H017	0.21	0.82	14.8	8.37	P059	1.27	2.18	15.3	10.45
H018	0.23	0.68	13.8	11.02	P060	0.47	1.81	14.7	7.95
H019	0.53	1.70	15.1	30.18	P061	0.57	1.46	16.5	19.34
Average		0.91		12.81	Average		1.64		14.43
St. Dev.		0.28		6.71	St. Dev.		0.32		6.57

Statistically, a strong trend shows that the porcine eyes can handle a larger pressure and a larger stress than human eyes, and that the human and porcine eyes are both stronger in dynamic situations than in static situations (Table 5). A p-value of less than 0.05 (5% confidence interval) indicates a statistically significant difference.

Table 5 Statistical analysis of data

Stress Test	P-Value	Analysis of Stress	Pressure Test	P-Value	Analysis of Pressure
Human Static vs Porcine Static	0.008	Porcine was stronger	Human Static vs Porcine Static	0.001	Porcine was stronger
Human Dynamic vs Porcine Dynamic	0.539	They were the same	Human Dynamic vs Porcine Dynamic	0.001	Porcine was stronger
Human Static vs Human Dynamic	0.008	Dynamic was stronger	Human Static vs Human Dynamic	0.001	Dynamic was stronger
Porcine Static vs Porcine Dynamic	0.045	Dynamic was stronger	Porcine Static vs Porcine Dynamic	0.001	Dynamic was stronger

For both quasi-static and dynamic tests, rupture primarily occurred on the equator (Table 6, Table 7).

Table 6 Static rupture location and corresponding thickness at rupture location

Static					
Human	Location	Thickness (mm)	Porcine	Location	Thickness (mm)
H009	Limbus	0.725	P035	Optic Nerve	1.6
H010	Equator	0.425	P036	Equator	0.625
H011	Equator	0.425	P037	Equator	0.625
H012	Equator	0.425	P038	Equator	0.625
H013	Equator	0.425	P039	Cornea	1.675
H020	Equator	0.425	P040	Equator	0.625
H021	Equator	0.425	P062	Equator	0.625
H023	Equator	0.425	P064	Equator	0.625
H024	Limbus	0.725	P065	Equator	0.625
H026	Equator	0.425	P067	Equator	0.625

Table 7 Dynamic rupture location and corresponding thickness at rupture location

Dynamic					
Human	Location	Thickness (mm)	Porcine	Location	Thickness (mm)
H002	Equator	0.425	P048	Equator	0.625
H003	Equator	0.425	P049	Cornea	1.675
H004	Limbus	0.725	P054	Equator	0.625
H005	Limbus	0.725	P055	Equator	0.625
H006	Equator	0.425	P056	Cornea	1.675
H008	Equator	0.425	P057	Equator	0.625
H014	Equator	0.425	P058	Equator	0.625
H017	Limbus	0.725	P059	Optic Nerve	1.6
H018	Equator	0.425	P060	Cornea	1.675
H019	Equator	0.425	P061	Equator	0.625

High-speed video and digital photo images of a typical equatorial rupture are shown (Figure 5), as are high-speed video and digital photo images of a rupture occurring at the limbus (Figure 6).

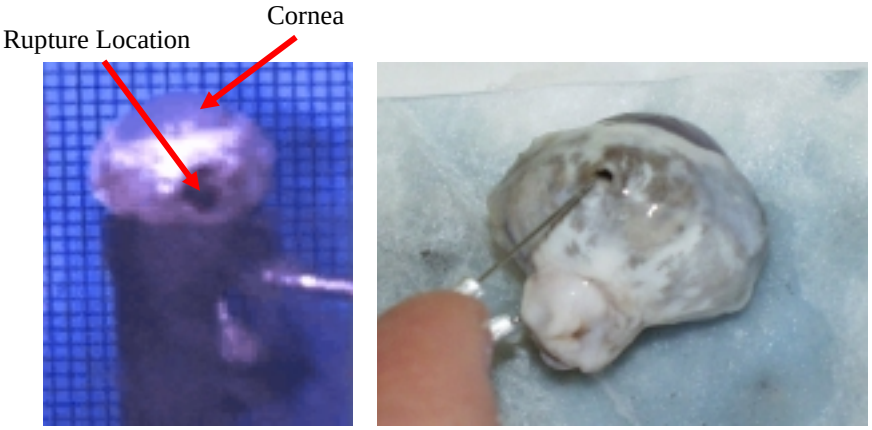

Figure 5 Pictures showing porcine ocular rupture at the equator during dynamic testing. High-speed video showing failure during testing (left) and post-test examination of the same eye (right).

Figure 6 Pictures showing porcine ocular rupture at the limbus during testing. High-speed video showing failure during testing (left) and post-test examination of the right eye (right).

Strain

Stress-strain relationships for two human static tests and two human dynamic tests are shown (Figures 7 through 10). The stress at each time was found and presented earlier in this report. The strain at each time was determined according to the change in radius with time (see Discussion). Because stress and strain were each known at every time throughout the event, stress and strain were easily correlated. The data were fit with a curve to approximate the stress-strain relationship, and the modulus of elasticity was calculated as the slope of the stress-strain curve. Because the slope changes with time, the modulus was calculated for every 0.02 in/in of strain.

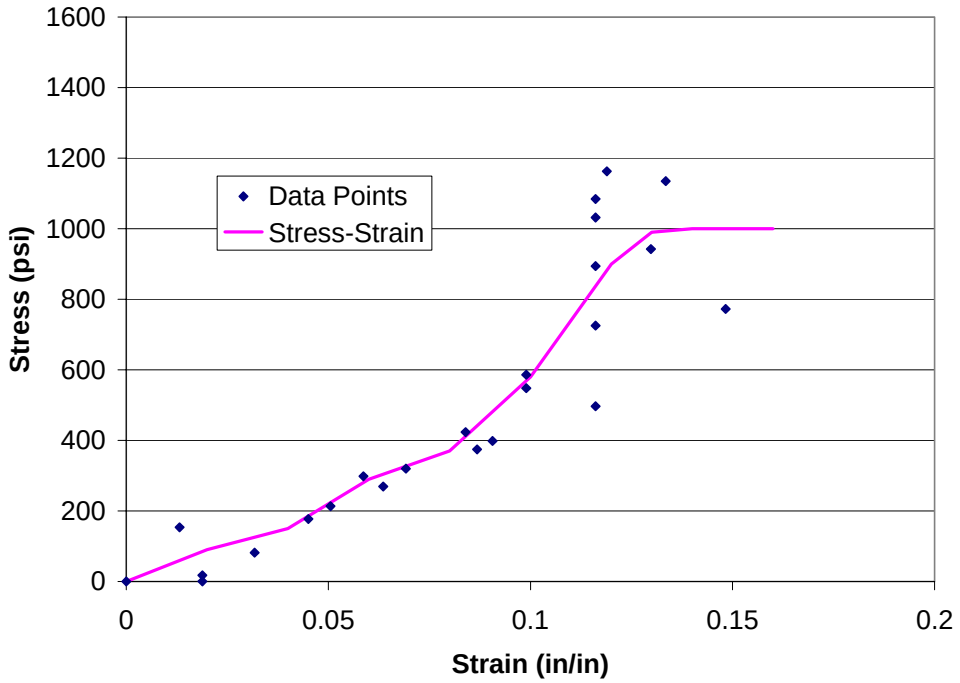

Figure 7 Stress-strain for human dynamic test 1

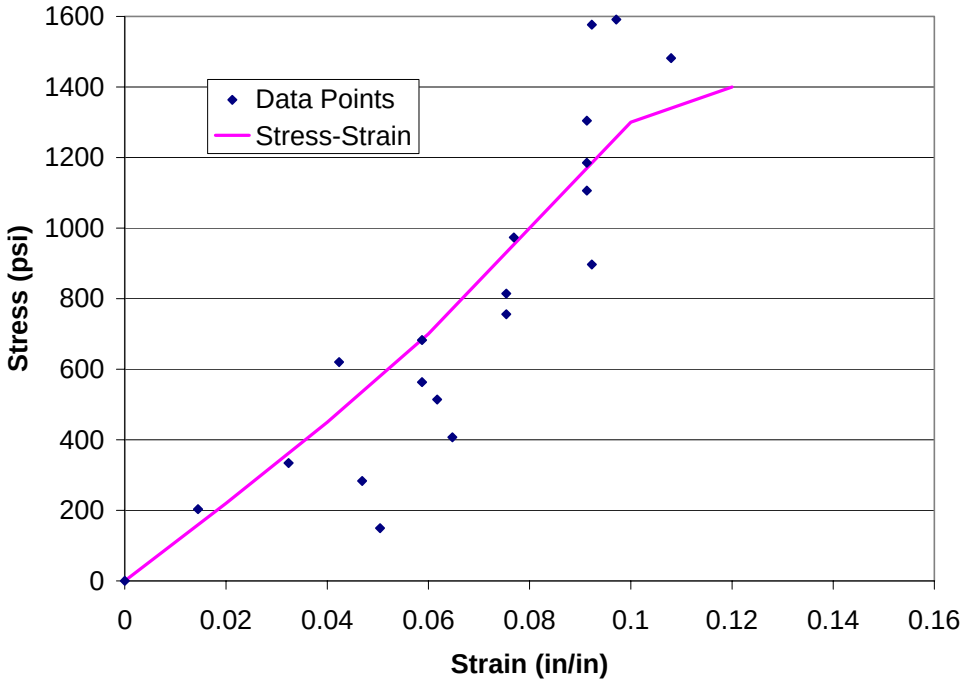

Figure 8 Stress-strain for human dynamic test 2

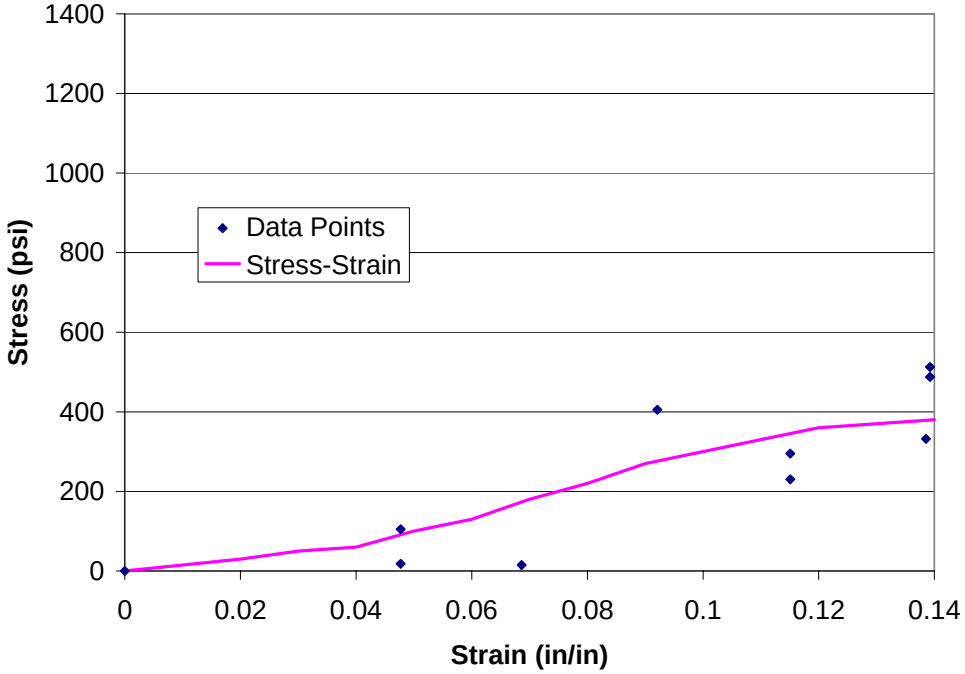

Figure 9 Stress-strain for human static test 1

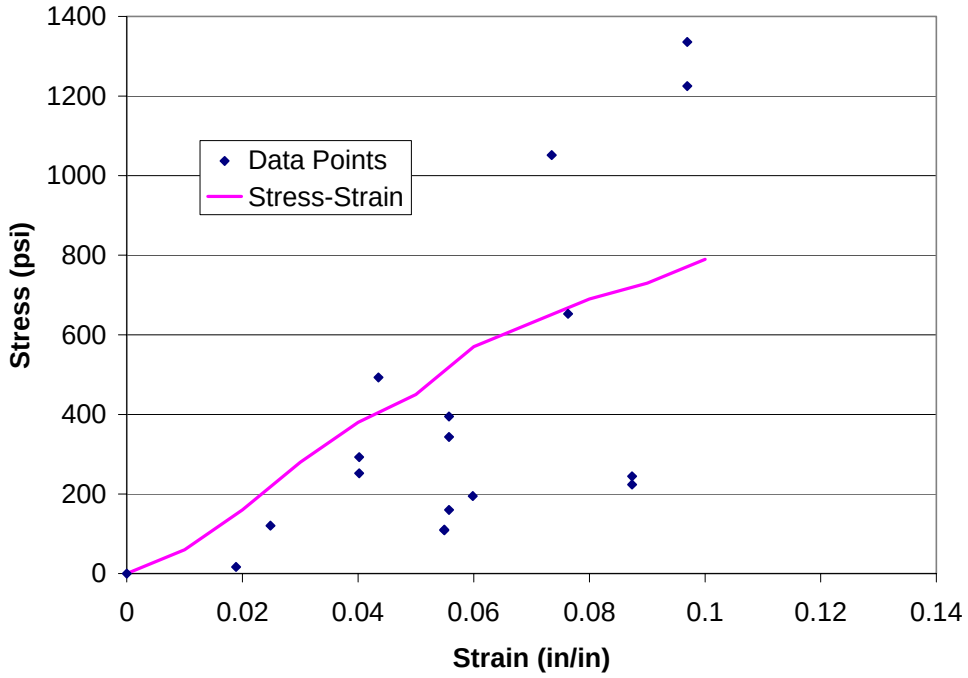

Figure 10 Stress-strain for human static test 2

Each of the slopes of the stress-strain curves presented above were analyzed to determine the modulus of elasticity. The modulus of elasticity is nonlinear, and initially increases until a strain of approximately 0.04in/in where the modulus begins to decrease. Values ranged from a maximum of approximately 5000psi for one test, to a maximum of 15,000psi for the three remaining tests.

Table 8 Human dynamic eye H017

Strain (in/in)	**Modulus of Elasticity (psi)**
0	0
0.02	4500
0.04	3000
0.06	7000
0.08	4000
0.1	10500
0.12	16000
0.13	9000
0.14	1000

Table 9 Human dynamic eye H018

Strain (in/in)	Modulus of Elasticity (psi)
0	0
0.02	11000
0.04	11500
0.06	12500
0.08	15000
0.1	15000
0.12	5000

Table 10 Human static eye H020

Strain (in/in)	Modulus of Elasticity (psi)
0	0
0.02	1500
0.03	2000
0.04	1000
0.05	4000
0.06	3000
0.07	5000
0.08	4000
0.09	5000
0.1	3000
0.11	3000
0.12	3000
0.13	1000
0.14	1000

Table 11 Human static eye H023

Strain (in/in)	Modulus of Elasticity (psi)
0	0
0.01	6000
0.02	8000
0.03	11000
0.04	11000
0.05	8500
0.06	9500
0.07	9000
0.08	6000
0.09	5000
0.1	5000

Discussion

Stress

Because biological tissue is rate-sensitive to loading, both quasi-static and dynamic tests were needed to gain a more complete understanding of the overall tissue behavior. At high rate loading, biological tissue can withstand a higher load, whereas with static or low rate loading, the tissue withstands a much lower load. Ramp-up on a typical human and porcine quasi-static test is shown (Figure 11). Quasi-static loading was achieved manually, and although the rates vary slightly between tests, the pressure was increased at a rate of approximately 1psi/s. For quasi-static loading, pressure drop-off shows on the graph immediately after rupture whereas with dynamic loading, pressure drop-off does not appear on the graph because of the quantity of time gathered during data collection. Only 1.6 seconds appears on the dynamic graph, but 200 seconds appear on the quasi-static graph. Data were collected for the dynamic case at 6000Hz to gather enough data over the rupture event to accurately determine the precise instant of rupture and corresponding rupture pressure. Therefore, only 1.6 seconds of data were collected. Because pressure was increased so slowly during the quasi-static tests, it was more important to gather a long string of data over a long period of time rather than a high acquisition rate over a short period of time.

Data were collected over the entire pressure ramp-up, including the rupture event. Eyes (quasi-statically and dynamically) ruptured during ramp-up, insuring that the recorded rupture event occurred at the maximum pressure.

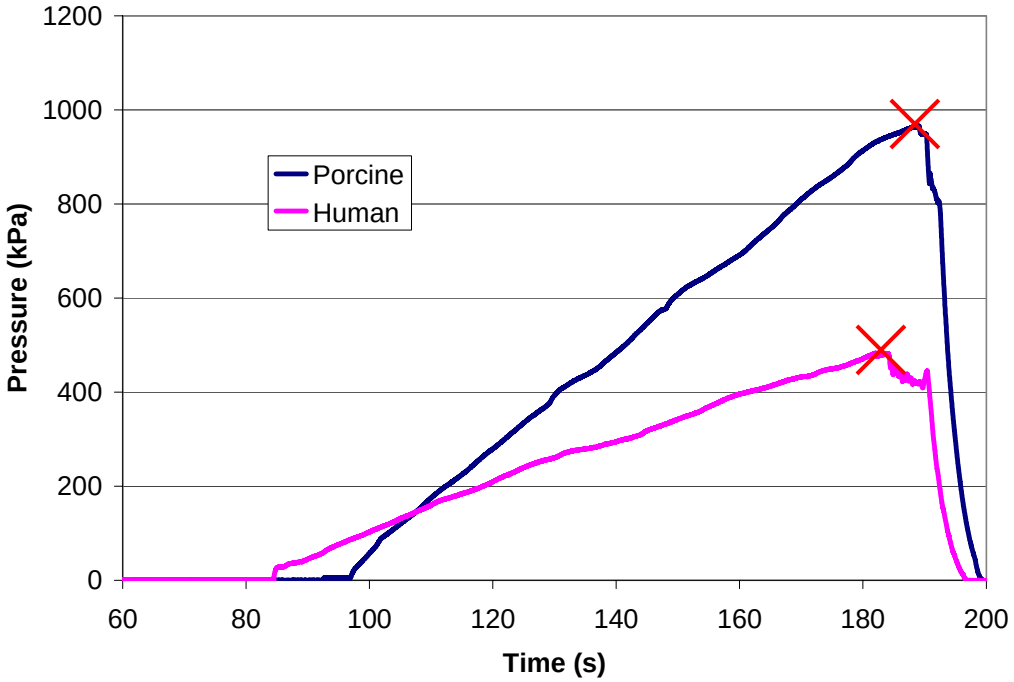

Figure 11 Quasi-static ramp-up for a typical human and porcine test showing rupture event

For high-rate (dynamic) loading, human eyes were found to rupture at a much lower pressure than average porcine rupture. Ramp-up on a typical human and porcine dynamic test is shown (Figure 12). It is not important that the lines do not lie on top of each other, as each globe rupture event was captured by the computer at a slightly different time relative to rupture. It can be seen, however, that the loading rates are equivalent between tests, and that globe rupture occurred within approximately half a second from pressure release for dynamic tests.

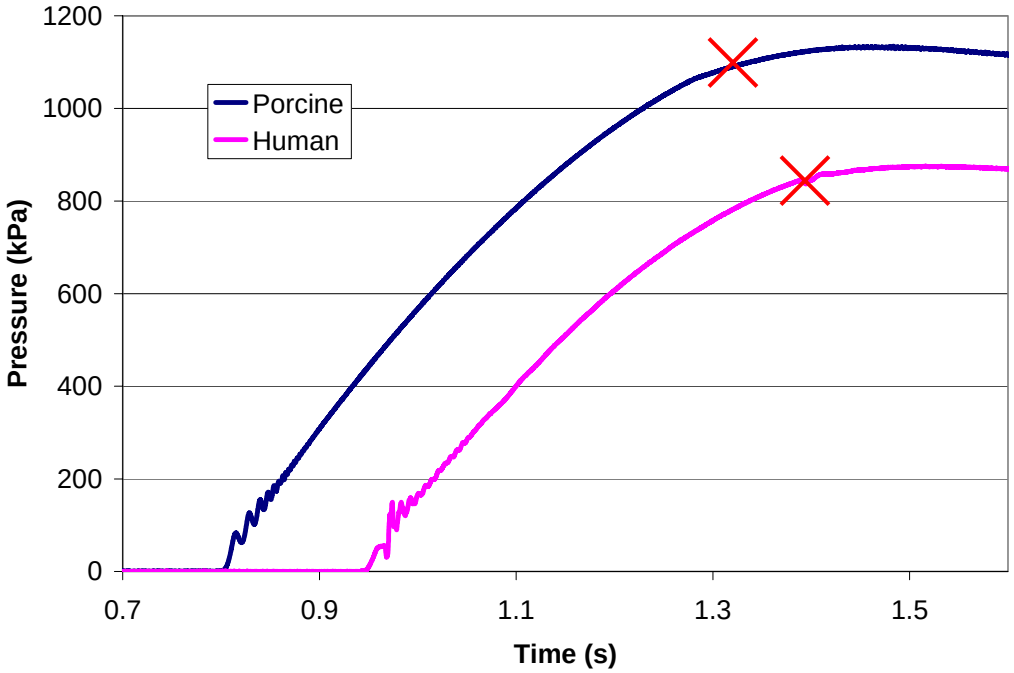

Figure 12 Dynamic ramp-up for a typical human and porcine test showing rupture event

Overall, human eyes were found to be much weaker than porcine eyes. The porcine eyes used were 6-9 months of age, and tested within 48 hours of slaughter. The human eyes, however, were between 55 and 87 years of age and were tested at varying times after death (between 1 and 4 months post-mortem). Human eyes are difficult to obtain, therefore all eyes that were available were used for testing, regardless of age of the subject or time after death. For this experiment, the data were analyzed by comparing differences between young porcine eyes with elderly human eyes. The human results are therefore expected to be lower in magnitude as compared to the porcine results, because tissues become less resilient and weaker with age. However, it is unclear as to how much of the difference can be attributed to age and how much of the difference is caused by species differentiation. Based on correlation testing between rupture pressure and time from death or rupture pressure and age, for humans, rupture pressure was not correlated with time from death after 22 days (Figure 13), or age for human eyes older than 55 years (Appendix F). This study did not include correlation testing for eyes younger than 55

years, or for eyes between 1 and 22 days after death, however, it is known that some postmortem degradation of tissues has occurred in the hours and days just after death.

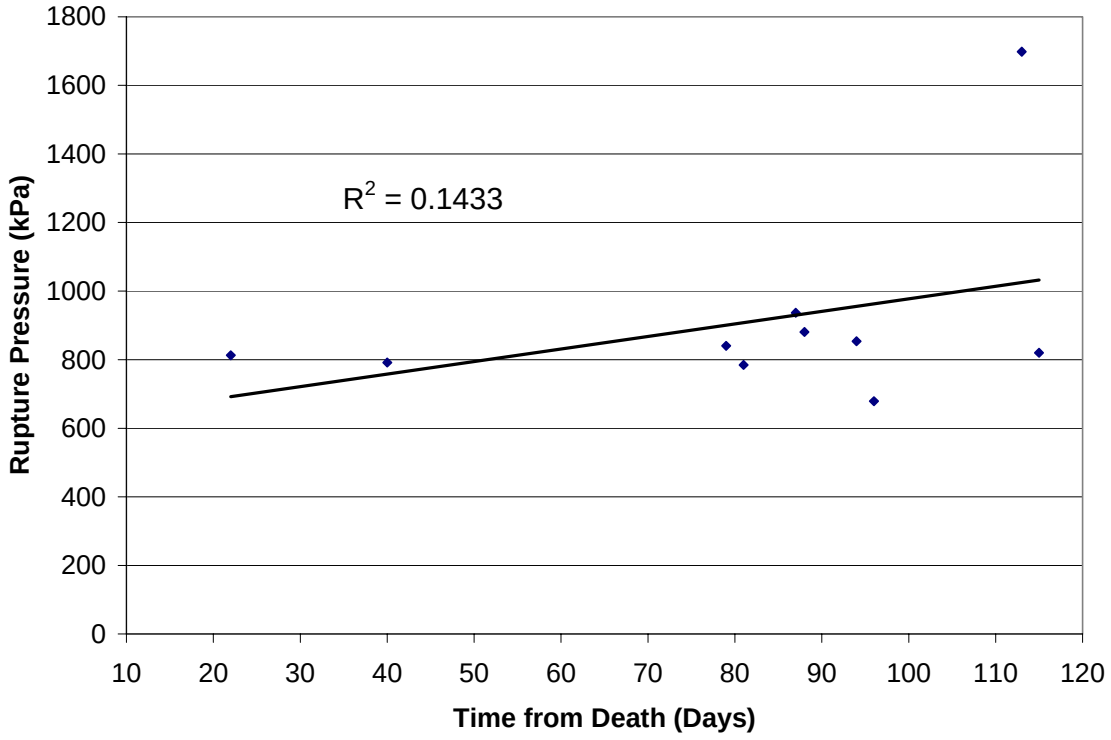

Figure 13 Example of non-correlation between rupture pressure and time from death for human dynamic testing

For both quasi-static and dynamic tests, rupture primarily occurred on the equator. This was expected because the equator is the location on the globe where the wall is the thinnest. Through histology, pigs were found to have an equatorial wall thickness of approximately 0.425 mm, whereas near the posterior pole of the eye the thickness is 1.275 mm. For humans, the thickness of the wall at the global equator is approximately 0.625 mm, whereas near the posterior pole of the eye the thickness is 1.6 mm. Based on the thickness at approximate rupture location and rupture pressure of each eye, the relationship for thin-walled spheres (Higdon, 1985) was employed to relate internal rupture pressure to yield stress for ocular tissues (Figure 14).

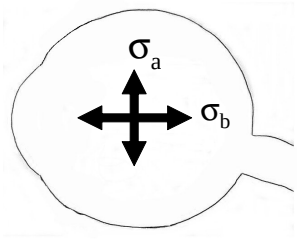

$\sigma_a = \sigma_b = Pr/2t$

P = internal pressure in a sphere

r = radius of the sphere

t = wall thickness

Figure 14 Stress on ocular tissues produced by an internal pressure

For human tissue, average stress for the quasi-static tests was found to be approximately 5.34MPa, whereas average stress for the dynamic tests was found to be 12.81MPa. Maximum stress for static loading was found to be 11.17MPa whereas maximum stress for dynamic loading was 30.18MPa. Static human results are well correlated with the previous data, where Uchio (1999) found the maximum stress to be approximately 9.4MPa with static material properties. Human dynamic results are slightly higher than the VTEM (Stitzel, 2002) where maximum stress with dynamic properties was found to be 23MPa. Porcine tissue average rupture stress was found to be 9.4MPa under static loading and 14.43MPa under dynamic loading. Maximum static stress for porcine tissue was 12.08MPa and maximum dynamic stress was found to be 26.01MPa. The porcine results are approximately 3MPa higher than previous studies (Table 12).

Table 12 Stress comparison

Test	Static Stress (MPa)	Dynamic Stress (MPa)
Uchio (1999)	9.4	----
Stitzel (2002)	----	23
Human Range	1.76 - 11.17	6.59 - 30.18
Average Human	5.34	12.81
Porcine Range	4.93 - 12.08	7.12 - 26.01
Average Porcine	9.38	14.43

The VTEM found peak pressures exceeding 2.1MPa for dynamic loading, and this study found similar pressures under dynamic loading. Although human rupture pressures lingered around 0.9MPa, porcine rupture pressures averaged 1.64MPa, with the maximum pressure at 2.18MPa. As shown, it is important to differentiate between tissue types and static versus dynamic failure properties before drawing conclusions from computer models or making predictions on injury criteria.

Strain

Strain was found by analyzing the radii at each pressure, and entering the data into the corresponding strain equation where r_1 is always the initial radius for each eye, r_2 is the radius at each corresponding pressure point, and ε is Lagrangian strain (Equation 2).

$$\varepsilon = (r_2 - r_1)/r_1 \qquad (2)$$

Stress and strain were then plotted together for the overall stress-strain relationship. Compared with the VTEM (2002) data, the stress-strain relationships found during testing had a lower slope (smaller E) as shown in Figure 15.

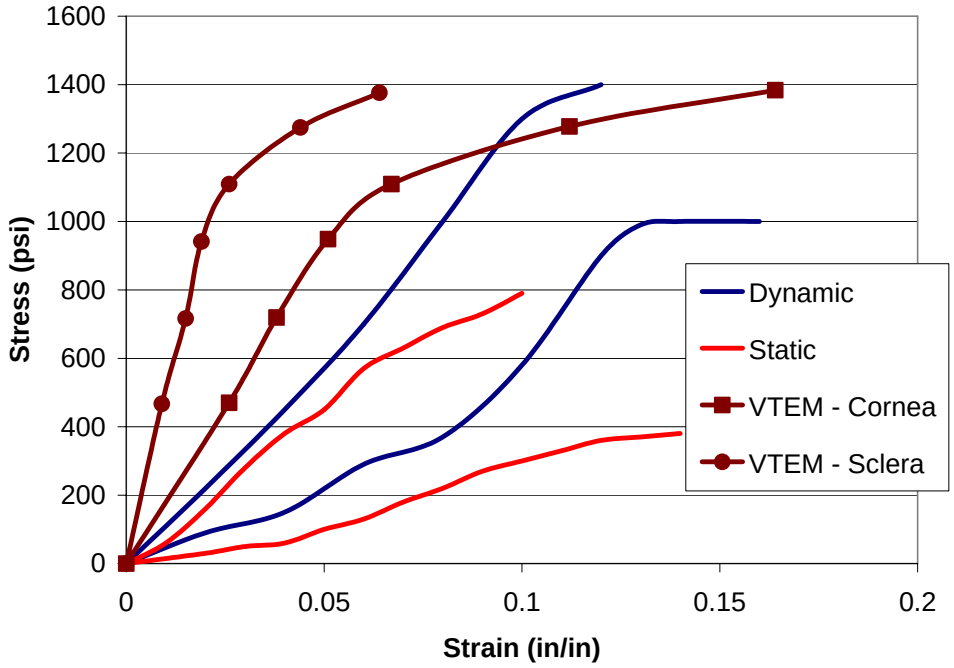

Figure 15 Stress-strain relationships for the 4 tests conducted in this experiment and the values used in the VTEM

Dynamically and statically, the stress-strain relationships have a lower slope than the Uchio (1999) uniaxial strip tests and predictions from the VTEM. The dynamic tests appear to have a sharper slope which tails off at the end, much like the VTEM stress-strain relationships, where the static tests have a fairly consistent slope throughout the curve.

Because the strain portion of this experiment was of an investigatory nature, some improvements in the process can be made. These stress-strain relationships could be better investigated using a higher resolution video, as the eye will only change approximately 6 pixels over the entire event. Additionally, a method that would allow the investigator to track the entire circumference of the eye over the pressurization event would be of interest, as the change in diameter of the eye depends on the exact choice for measurement location.

Conclusions

Through this study, a pressure system was built to analyze quasi-static and dynamic rupture pressure of human and porcine eyes. Rupture stress and the stress-strain relationship for the globe of the human eye are research areas of little information, but are critical when analyzing globe properties computationally. Accurate failure properties for rupture stress were found to be 5.34MPa on average for human tissue and 9.38MPa on average for porcine tissue under static loading, whereas stresses for the dynamic tests were found to be 12.81MPa on average for human tissue and 14.43MPa on average for

porcine tissue. Maximum stresses correlate well with previous data with static properties (9.4MPa) and dynamic properties (23MPa). Values for the elastic modulus, E, were slightly lower than the published values used by Uchio (1999) and Stitzel (2002) for the sclera. The lower values found for the stress-strain relationships may be attributed to real-life testing, where localized weaknesses in the globe and relative accuracy of the method of measuring globe diameter affect the outcome.

Rupture pressure is now known and may be of interest to clinical ophthalmologists, and the corresponding ultimate stress at rupture can be used in computer models for convenient, versatile experimentation to evaluate potential dangers to the eye. Now that rupture can be accurately determined, this information can be used to evaluate the effectiveness of safety systems designed to protect eyesight in automotive, sports, and military applications.

References

Bass C, Davis M, Stitzel J, Duma S (2002) Airbag interaction with night vision goggles. Report to the United States Army Aeromedical Research Laboratory, Ft Rucker, Alabama.

Biehl JW, Valdez J, Hemady RK, Steidl SM, Bourke DL (1999) Penetrating eye injury in war. Military Medicine 164(11):780-784.

Burnstein Y, Klapper D, Hersh PS. "Experimental globe rupture after excimer laser photorefractive keratectomy." Arch Ophthalmol 113(1995):1056-1059.

Chisholm L (1969) Ocular injury due to blunt trauma. Applied Therapeutics 11(11): 597-598.

Doswald-Beck EL (1993) Blinding weapons. Geneva, International Committee of the Red Cross.

Duma SM, Jernigam MV, Stitzel JD, Herring IP, Crowley JS, Brozoski FT, Bass CR. "The effect of frontal air bags on eye injury patterns in automobile crashes." Arch Ophthalmol 120 (2002):1517-1522.

Duma SM, Kress TA, Porta DJ, Woods CD, Snider JN, Fuller PM, Simmons RJ (1996) Airbag-induced eye injuries: a report of 25 cases. The Journal of Trauma: Injury, Infection, and Critical Care 41(1):114-119.

Ghafouri A, Burgess SK, Hrdlicka ZK, Zagelbaum BM (1997) Air bag - related ocular trauma. American Journal of Emergency Medicine 15(4): 389-392.

Heier JS, Enzenauer RW, Wintermeyer SF, et al (1993) Ocular injuries and diseases at a combat support hospital in support of Operations Desert Shield and Desert Storm. Arch Ophthalmol 111:795-798.

Higdon A, Ohlsen EH, Stiles WB, Weese JA, Riley WF (1985) Mechanics of Materials, Fourth Edition, John Wiley & Sons.

Kisielewicz LT, Kodama N, Ohno S, Uchio E (1998) Numerical prediction of airbag caused injuries on eyeballs after radial keratotomy. SAE International Congress and Exposition.

Muller-Jensen K, Hollweck W (1970) Serious eye injuries produced by windshield damage-an actual problem in ophthalmology. SAE Stapp Car Crash Conference Proceedings 700912:388-396.

Power ED, Stitzel JD, Duma SM, Herring IP, West RL (2002) Investigation of ocular injuries from high velocity objects in an automobile collision. SAE Technical Paper Series 2002-01-0027:1-8.

Parver LM (1986) Eye trauma: the neglected disorder. Archives of Ophthalmology 104:1452-1453.

Pinheiro MN, Bryant MR, Tayyanipour R, Nassaralla BA, Wee WR, McDonnell PJ. "Corneal integrity after refractive surgery." Ophthalmology 102(1995):297-301).

Stein JD, Jaeger EA, Jeffers JB (1999) Air bags and ocular injuries. Tr. Am. Ophth. Soc.97:59-82.

Stitzel JD, Duma SM, Cormier JM, Herring IP. "A nonlinear finite element model of the eye with experimental validation for the prediction of globe rupture." Stapp Car Crash Journal 46 (2002).

Uchio E, Ohno S, Kudoh J, Aoki K, Kisielewicz LT (1999) Simulation model of an eyeball based on finite element analysis on a supercomputer. Br J Ophthalmol 83:1106-1111.

Vichnin MC, Jaeger EA, Gault JA, Jeffers JB (1995) Ocular injuries related to air bag inflation. Ophthalmic Surg Lasers 26: 542-548.

Vinger PF, Duma SM, Crandall JR (1999) Baseball hardness as a risk factor for eye injuries. Archives of Ophthalmology 117:354-358.

Young B, Heath JW (2000) Wheater's Functional Histology: A Text and Colour Atlas. Harcourt Publishers Limited.